INSTITUTE FOR FUSION STUDIES

DOE/ET-53088-512 IFSR #512

Vlasov-Maxwell System:
2-D Equilibria, Reversed Field Pinches

S.M. MAHAJAN
International Centre for Theoretical Physics
Trieste, Italy and
IFS-UT-Austin, Austin, TX 78712

W.Q. LI
IFS-UT-Austin, Austin, TX 78712

and A. SEN
International Centre for Theoretical Physics
Trieste, Italy

August 1991

THE UNIVERSITY OF TEXAS

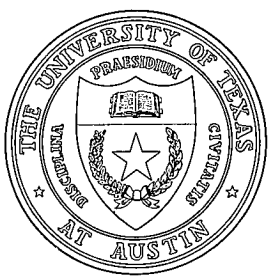

AUSTIN

Vlasov-Maxwell System: 2-D Equilibria, Reversed Field Pinches

S.M. Mahajan
International Centre for Theoretical Physics
Trieste, Italy
Institute for Fusion Studies
The University of Texas at Austin
Austin, Texas 78712

W.Q. Li
Institute for Fusion Studies
The University of Texas at Austin
Austin, Texas 78712

and

A. Sen*
International Centre for Theoretical Physics
Trieste, Italy

Abstract

Exact solutions to the Vlasov-Maxwell system in the two dimensional circular cylindrical model are presented. The magnetic surfaces are shifted circles for the $m = 1$ case, where the shift is determined by a parameter ϵ; $\epsilon = 0$ gives concentric circles and represents 1-D solutions. For $m \geq 2$ cases, the solutions are singular at the origin and the magnetic surfaces contain islands and separatrices. An improved one dimensional model with currents in both the axial and azimuthal directions is also presented. It is shown that this simple finite pressure model can yield field reversed equilibria in the presence of appropriate boundary constraints.

*Permanent Address: I.P.R, Ahmedabad, India

I. Introduction

In this paper, we extend the investigation[1,2] of the solutions to the Vlasov-Maxwell system, to consider some exact two dimensional equilibria as well as an improved one dimensional model equilibrium that can provide a simple representation of a field reversed pinch plasma. The motivation, as before,[1,2] is to arrive at a more realistic description of laboratory plasmas through the Vlasov approach which permits proper inclusion of density and temperature gradients in a natural way.[2] Our results are derived on the basis of the infinite series distribution function which has been shown to be an exact solution of the Vlasov equation. We briefly review the properties of this distribution function in Sec. II. The expansion coefficients in the infinite series are proportional to powers of the parameter, $\lambda = u_{0\alpha}/v_{0\alpha}$, where $u_{0\alpha}$ and $v_{0\alpha}$ are, respectively, the drift and thermal speeds of the αth species. For laboratory plasmas where $\lambda \ll 1$, this series can be readily truncated and we derive a set of differential equations relating the density (g) and temperature (ψ^2) profiles to the electromagnetic fields. We present exact two dimensional solutions to these equations and discuss their features in Sections III and IV. The magnetic configurations corresponding to these solutions are shifted circular surfaces for the $m = 1$ case (where m is the azimuthal mode number) and chains of magnetic islands separated by separatrices for the $m \geq 2$ cases. The latter solutions are also singular at the origin.

In Sec. V, we consider a one dimensional cylindrical plasma with currents in both the axial ($\hat{z}$) and azimuthal ($\hat{\theta}$) directions. The distribution function is suitably modified to include a term proportional to p_θ, the canonical angular momentum, and following the usual truncation procedure, a set of coupled equations are again obtained relating the equilibrium plasma profiles to the electromagnetic fields. These equations also admit exact solutions which are an interesting extension of simpler solutions obtained previously.[1,2] Next we in-

troduce an external B_z field modeled by a current at the boundary. The solutions of the modified model equations are then seen to display field reversal phenomena. These equilibrium states resemble 'Relaxed' states of reversed field pinches and can be viewed as the kinetic analog (with finite pressure and pressure gradients) of the single fluid states discussed in the literature.[3] An example of a numerical plot of a $F - \Theta$ curve is shown for this model pinch equilibrium. Section VI contains a brief discussion of our results, their implications and directions for future work.

II. Solutions in Terms of Invariants

We begin by constructing a distribution function describing the plasma with the density and temperature gradients. The function is exactly the same as that in Refs. 1 and 2. But, here, we deal with the problem in a two dimensional cylindrical geometry. The plasma, embedded in a strong external field $B_0\,\hat{z}$, has current flowing only in the $\hat{z}$ direction. The equilibrium now depends both on r and θ allowing the axial current to produce a new general self-consistent magnetic field $\mathbf{B} = B_r\hat{r} + B_\theta\hat{\theta}$. The infinite series distribution function[1,2] is

$$f_\alpha = \frac{n_{0\alpha}g_\alpha}{\pi^{3/2}v_{0\alpha}^3\psi_\alpha^3}\left[1 + \frac{2u_{0\alpha}}{v_{0\alpha}}\sum_{n=1}^{\infty}\sum_{m=0}^{\infty}C_{nm}^{\alpha}\left(\frac{v_z}{v_{0\alpha}}\right)^n\left(\frac{v}{v_{0\alpha}\psi_\alpha}\right)^{2m}\right]\exp\left(-\frac{v^2}{v_{0\alpha}^2\psi_\alpha^2}\right), \qquad (1)$$

where the density $n_\alpha = n_{0\alpha}g_\alpha$, the thermal velocity $v_\alpha = (2T_\alpha/m_\alpha)^{1/2} = v_{0\alpha}\psi_\alpha$, with g_α and ψ_α being the profile factors, and $u_{0\alpha}$ is a measure of the drift velocity in the $\hat{z}$ direction.

We first show that the choice of C_{nm}'s which make the distribution function, Eq. (1), solve the Vlasov equations also allows f_α to be expressed in terms of the constants of the motion. The derivation is simply a two dimensional version of the one given in the Appendix of Ref. 2. Substituting Eq. (1) into the steady-state Vlasov equation (describing the equilibrium Z pinch) yields the following general relationships for C_{nm}^{α} by equating power of v_z and v,

$$\mathbf{v}\cdot\nabla\left[\ln\left(\frac{g_\alpha}{\psi_\alpha^3}\right) - C_{10}^{\alpha}h_\alpha A_z\right] = 0\,, \qquad (2)$$

$$\left(\frac{v}{v_{0\alpha}\psi_\alpha}\right)^2 \mathbf{v}\cdot\nabla\left[2\ln\left(\psi_\alpha\right) - C_{11}^\alpha h_\alpha A_z\right] = 0 \ , \tag{3}$$

and

$$C_{nm}^\alpha = \frac{t^{n-1}}{n!m!}\sum_{s=0}^{m}(-1)^s(C_{10}^\alpha - sC_{11}^\alpha)^n D_{ms}$$

$$= \frac{t^{n-1}}{n!m!}\sum_{s=0}^{m}(-1)^s(1-s\beta_\alpha)^n D_{ms} \ , \tag{4}$$

where $h_\alpha = (q_\alpha u_{0\alpha})/(cT_{0\alpha})$, $t = 2u_{0\alpha}/v_{0\alpha}$, and $D_{ms} = m!/[(m-s)!s!]$ for $m \geq 0$ and $s \geq 0$. The recurrence relation Eq. (4) expresses the fact that all nonzero C_{nm}'s are expressible in terms of C_{10}^α and C_{11}^α. Without any loss of generality we choose $C_{10}^\alpha = 1$ (any other value can be absorbed in the redefinition of $u_{0\alpha}$, and appropriate scaling of C_{nm}^α) and put $C_{11}^\alpha = \beta_\alpha$. The summation from $m = 0$ to $m = \infty$ in Eq. (1) is thus given by (see the Appendix of Ref. 2)

$$\sum_{m=0}^{\infty} C_{nm}^\alpha z_\alpha^m = \frac{t^{n-1}}{n!}\exp(z_\alpha)\sum_{s=0}^{\infty}\frac{(-z_\alpha)^s}{s!}(1-s\beta^\alpha)^n \ , \tag{5}$$

where $z_\alpha = [v/(v_{0\alpha}\psi_\alpha)]^2$. Equations (2) and (3) are now integrated to yield

$$\frac{g_\alpha}{\psi_\alpha^3} = e^{h_\alpha A_z} \ , \tag{6}$$

and

$$\psi_\alpha^2 = e^{\beta_\alpha h_\alpha A_z} \ . \tag{7}$$

which along with Eq. (5), and the definitions $H_\alpha = \frac{1}{2}m_\alpha v^2$, $p_{z\alpha} = m_\alpha v_z + (q_\alpha/c)A_z(r,\theta)$ help us rewrite Eq. (1) (see the Appendix of Ref. 2) entirely in terms of the invariants H_α and $p_{z\alpha}$,

$$f_\alpha = \frac{n_{0\alpha}}{\pi^{3/2}v_{0\alpha}^3}\exp\left(\frac{u_{0\alpha}}{T_{0\alpha}}p_{z\alpha}\right)\exp\left[-\frac{H_\alpha}{T_{0\alpha}}\exp\left(-\beta_\alpha\frac{u_{0\alpha}}{T_{0\alpha}}p_{z\alpha}\right)\right] \ . \tag{8}$$

Note that $\beta_\alpha = 0$ reduces Eq. (8) to the standard drifting Maxwellian with a constant temperature $T_{0\alpha} \neq 0$. It is also clear from Eq. (8) that r and θ dependence of the distribution function can come only through the canonical momentum $p_{z\alpha}$. Expressing the exact solution

(1) into the form (8), which is an explicit function of the constants of the motion, constitutes the main result of this section.

III. 2-D Solutions to Vlasov-Maxwell System

We consider a plasma which has a current in the axial ($\hat{z}$) direction and whose equilibrium profiles are a function of (r, θ) in the cylindrical geometry. The equilibrium is obtained by solving the $\hat{z}$ component of Ampére's law

$$\nabla^2 A_z = -\frac{4\pi}{c} J_z \ , \tag{9}$$

where J_z is to be calculated using the solution of the Vlasov equation given in Sec. II. For simplicity, we calculate J_z only to $O(u_{0\alpha}/v_{0\alpha} = \lambda \ll 1)$

$$J_z = e n_0 u_{0e} \left(\frac{5\beta}{2} - 1 \right) (1+\tau) g \psi^2 = -chp \ , \tag{10}$$

where $\tau = T_{0i}/T_{0e}$, $h = h_e(5\beta/2 - 1)$, and $p = p_0 g \psi^2$ is the pressure with $p_0 = n_0 T_{0e}(1+\tau)$ being the pressure at the plasma center ($r = 0$). In deriving Eq. (10), we have assumed that $g_i = g_e = g$ (quasineutrality) and $\psi_i = \psi_e = \psi$ (for long-lived equilibria), implying $T_{0i}/T_{0e} = -u_{0i}/u_{0e}$ and $\beta_i = \beta_e = -\beta$. Making use of Eqs. (6) and (7), and defining

$$h\Phi = -h_e \left(\frac{5\beta}{2} - 1 \right) A_z \ , \tag{11}$$

where $\Phi = -A_z$ is the magnetic surface function, Ampére's law [Eq. (9)] can be cast as

$$\frac{1}{R}\frac{\partial}{\partial R} R \frac{\partial h\Phi}{\partial R} + \frac{1}{R^2}\frac{\partial^2 h\Phi}{\partial \theta^2} = -(2r_0^2/\delta_1^2) e^{h\Phi} = -8m^2(1-\epsilon^2) e^{h\Phi} \ , \tag{12}$$

where $R = r/r_0$, $r_0 = 2\delta_1 m (1-\epsilon^2)^{1/2}$, and the scale length

$$\delta_1 = \left[\frac{2\pi n_0 e^2}{T_{0e}} \frac{u_{0e}^2}{c^2} \left(\frac{5\beta}{2} - 1 \right)^2 (1+\tau) \right]^{-1/2} = \frac{1}{|h|\,(2\pi p_0)^{1/2}} \ . \tag{13}$$

Equation (12) admits exact solutions[4-6] of the form

$$h\Phi = -2 \ln[R^{1+m} + R^{1-m} + 2\epsilon R \cos(m\theta)] \ , \tag{14}$$

yielding the following expressions for the relevant physical quantities:

$$g\psi^2 = e^{h\Phi} = \left\{ \frac{R^{(m-1)}}{[R^{2m} + 2\epsilon R^m \cos(m\theta) + 1]} \right\}^2 , \tag{15}$$

$$g = \left[\frac{R^{(m-1)}}{R^{2m} + 2\epsilon R^m \cos(m\theta) + 1} \right]^{2(3\beta-2)/(5\beta-2)} , \tag{16}$$

$$\psi^2 = \left[\frac{R^{(m-1)}}{R^{2m} + 2\epsilon R^m \cos(m\theta) + 1} \right]^{4\beta/(5\beta-2)} , \tag{17}$$

$$J_z = -chp = \left(\frac{p_0 c^2}{2\pi\delta_1^2} \right)^{1/2} \left\{ \frac{R^{(m-1)}}{[R^{2m} + 2\epsilon R^m \cos(m\theta) + 1]} \right\}^2 , \tag{18}$$

$$B_r = \left[\frac{\pi p_0}{2(1-\epsilon^2)} \right]^{1/2} \left[\frac{4\epsilon R^{(m-1)} \sin(m\theta)}{R^{2m} + 2\epsilon R^m \cos(m\theta) + 1} \right] , \tag{19}$$

and

$$B_\theta = \left[\frac{2\pi p_0}{m^2(1-\epsilon^2)} \right]^{1/2} \left[\frac{(1+m)R^{(2m-1)} + (1-m)R^{-1} + 2\epsilon R^{(m-1)} \cos(m\theta)}{R^{2m} + 2\epsilon R^m \cos(m\theta) + 1} \right] , \tag{20}$$

where the self-consistent magnetic field, B_θ, has the singularity at $R = 0$ (or $r = 0$) for $m \geq 2$, and ϵ lies in the range, $0 \leq \epsilon < 1$. In deriving Eqs. (18) to (20), we have used $-h = |h|$. The square of the magnitude of the magnetic field,

$$B^2 = \left[\frac{2\pi p_0}{m^2(1-\epsilon^2)} \right] \left\{ \frac{[(1+m)R^{(2m-1)} + (1-m)R^{-1}]^2 + 4\epsilon R^{(m-2)} \cos(m\theta)[(1+m)R^{2m} + (1-m)]}{[R^{2m} + 2\epsilon R^m \cos(m\theta) + 1]^2} \right.$$

$$\left. + \frac{4\epsilon^2 R^{2(m-1)}[1 + (m^2-1)\sin^2(m\theta)]}{[R^{2m} + 2\epsilon R^m \cos(m\theta) + 1]^2} \right\} , \tag{21}$$

will be used in the next section to calculate the magnetic energy.

Note that, in the limit $\epsilon = 0$, the solutions reduce to the 1-D case:

$$g = \left[\frac{R^{(m-1)}}{1 + R^{2m}} \right]^{2(3\beta-2)/(5\beta-2)} , \tag{22}$$

$$\psi^2 = \left[\frac{R^{(m-1)}}{1+R^{2m}}\right]^{4\beta/(5\beta-2)} , \tag{23}$$

$$J_z = \left(\frac{p_0 c^2}{2\pi\delta_1^2}\right)^{1/2}\left[\frac{R^{(m-1)}}{1+R^{2m}}\right]^2 \tag{24}$$

$$B_r = 0 , \tag{25}$$

and

$$B_\theta = \left(\frac{2\pi p_0}{m^2}\right)^{1/2}\left[\frac{(1-m)R^{-1}+(1+m)R^{(2m-1)}}{1+R^{2m}}\right] . \tag{26}$$

Thus, the 1-D solutions shown in Refs. 1 and 2 are only a special case ($m = 1$) of the solutions Eqs. (22)–(26). For $m \geq 2$, the magnetic field, B_θ, is singular at the center.

IV. Numerical results

A. $m = 1$ mode

In this section, we start to discuss the new solutions. We first consider the $m = 1$ case, and illustrate the contours of the magnetic surface function for different values of ϵ. It is shown, from Figs. 1, 2, and 3, that the structures of the contours are circles with their centers shifted toward the negative $\widehat{X}$ direction. We can understand this from Eq. (14), which takes the form:

$$\Phi = -\frac{2}{h}\ln(\sigma) , \tag{27}$$

where

$$\sigma = \frac{1}{4(1-\epsilon^2)}\left\{\left[X + 2\epsilon(1-\epsilon^2)^{1/2}\right]^2 + Y^2\right\} + 1 - \epsilon^2 , \tag{28}$$

with $X = r\cos(\theta)/\delta_1$ and $Y = r\sin(\theta)/\delta_1$. Clearly, the shapes are circles with centers at $X = -2\epsilon(1-\epsilon^2)^{1/2}$ and $Y = 0$, becoming concentric for $\epsilon = 0$. The centers shift to a maximum distance $X_{\max} = -1$ [$\epsilon = 2^{-(1/2)}$], then shift back toward the origin.

We also calculate the total plasma energy (K), and the magnetic energy (M) associated with these states,

$$K = \int_0^{r_p}\int_{-\pi}^{\pi}\frac{3}{2}nTrdrd\theta = \int_0^{\xi_p}\widehat{K}\xi d\xi , \tag{29}$$

and

$$M = \int_0^{r_p} \int_{-\pi}^{\pi} \frac{B^2}{8\pi} r dr d\theta = \int_0^{\xi_p} \widehat{M} \xi d\xi \ , \tag{30}$$

where $\xi = r/\delta_1$ and $\xi_p = r_p/\delta_1$, with r_p being the plasma radius. We plot $\widehat{K}$ and $\widehat{M}$ with respect to ξ in Figs. 4 and 5 respectively. For $\epsilon = 0$, representing the ordinary situation, the plasma pressure (or $\widehat{K}$) peaks at the plasma center and decays toward the edge, while the magnetic energy increases from zero (at $r = 0$) to a maximum value, and then decreases toward the edge. For larger ϵ (for example, $\epsilon = 0.6$ or 0.7), the magnetic energy begins with a larger value at the origin, forms a well around a particular region, and then decays toward the edge. The pressure clearly peaks near the location of the well, implying that the plasma is displaced from the center for larger ϵ.

B. $m \geq 2$ modes

All $m \geq 2$ solutions are singular at the origin. Figures 6-8 display the contours of the magnetic flux function for different values of ϵ. The crowded contours near the origin represent the singularity, and the magnetic islands and X points are clearly visible.

Figures 9 and 10 show the plots of the plasma and magnetic pressure with respect to ξ. To illustrate the results, we choose $m = 2$ as an example. The magnetic pressure is singular at $r = 0$. thus, no plasma exists there. The plasma clearly peaks near the region, where the magnetic pressure well is formed.

V. Pinch Equilibria; Field Reversal

In this section, we consider a further improvement in the pinch model by inclusion of an azimuthal current in the equilibrium. The motivation is to arrive at a better representation of laboratory devices like the reversed field pinches. However, for simplicity we restrict ourselves to one-dimensional cylindrical geometry. We once again start from the distribution

function of Sec. II, but modify it to include a term proportional to p_θ. It is given by

$$f_\alpha = \frac{n_{0\alpha}}{\pi^{3/2} v_{0\alpha}^3} \exp\left(\frac{u_{0\alpha}}{T_{0\alpha}} p_{z\alpha} + \frac{w_{0\alpha}}{T_{0\alpha}} p_{\theta\alpha}\right) \exp\left[-\frac{H_\alpha}{T_{0\alpha}} \exp\left(-\beta_\alpha \frac{u_{0\alpha}}{T_{0\alpha}} p_{z\alpha}\right)\right] , \tag{31}$$

where α denotes each plasma species, $u_{0\alpha}$ and $w_{0\alpha}$ are, respectively, the constant drift and angular velocities in the $\hat{z}$ and $\hat{\theta}$ directions, β_α measures the effect of the temperature gradient, and $p_{z\alpha} = m_\alpha v_z + (q_\alpha/c) A_z(r)$ and $p_{\theta\alpha} = m_\alpha r v_\theta + (q_\alpha/c) r A_\theta(r)$ are the canonical momenta. The plasma, thus, produces the self-consistent magnetic field $\mathbf{B} = B_z \hat{z} + B_\theta \hat{\theta}$.

Letting β_α equal to zero reduces Eq. (31) to the ordinary displaced Maxwellian distribution function.

For simplicity, we consider the problem only to order $\mathcal{O}(u_{0\alpha}/v_{0\alpha})$ and $\mathcal{O}(l w_{0\alpha}/v_{0\alpha})$, where l is the scale length of the system considered. This reduces Eq. (31) to

$$f_\alpha = \frac{n_{0\alpha}}{\pi^{3/2} v_{0\alpha}^3} \frac{g_\alpha}{\psi_\alpha^3} \exp\left(-\frac{v^2}{v_{0\alpha}^2 \psi_\alpha^2}\right) \left[1 + \frac{2 u_{0\alpha} v_z}{v_{0\alpha}^2} \left(1 + \beta_\alpha \frac{v^2}{v_{0\alpha}^2 \psi_\alpha^2}\right) + \frac{2 r w_{0\alpha} v_\theta}{v_{0\alpha}^2}\right] , \tag{32}$$

where g_α and ψ_α are the density and temperature profiles and are given by

$$g_\alpha = \exp\left[h_\alpha \left(1 + \frac{3\beta_\alpha}{2}\right) A_z + \tilde{h}_\alpha r A_\theta\right] , \tag{33}$$

and

$$\psi_\alpha^2 = \exp\left(h_\alpha \beta_\alpha A_z\right) , \tag{34}$$

with $\tilde{h}_\alpha = (q_\alpha w_{0\alpha})/(c T_{0\alpha})$. Further, if we assume that $g_i = g_e = g$ (quasineutrality) and $\psi_i = \psi_e = \psi$ (for long-lived equilibria), then

$$-\frac{u_{0i}}{u_{0e}} = -\frac{w_{0i}}{w_{0e}} = \frac{T_{0i}}{T_{0e}} = \tau . \tag{35}$$

To derive the relevant equations, we start from the axial and azimuthal components of Ampére's law

$$\frac{1}{r}\frac{d}{dr} r \frac{dA_z}{dr} = -\frac{4\pi}{c} J_z , \tag{36}$$

and

$$\frac{d}{dr}\frac{1}{r}\frac{d}{dr}rA_\theta = -\frac{4\pi}{c}J_\theta \ , \tag{37}$$

with currents J_z and J_θ calculated by using Eqs. (32) and (35),

$$J_z = n_0 e u_{0e}\left(\frac{5}{2}\beta - 1\right)(1+\tau)g\psi^2 = -chp \ , \tag{38}$$

$$J_\theta = -n_0 e r w_{0e}(1+\tau)g\psi^2 = -crh_0 p \ , \tag{39}$$

where $p = p_0 g\psi^2$, and $h_0 = -\tilde{h}_e$. With the definitions

$$P = -hA_z \ , \tag{40}$$

$$Q = -h_0 r A_\theta \ , \tag{41}$$

$$\delta_0 = \left[\frac{\pi n_0 e^2}{T_{0e}}\frac{u_{0e}^2}{c^2}\left(\frac{5\beta}{2} - 1\right)^2(1+\tau)\right]^{-1/2} = \frac{1}{|h|\,(\pi p_0)^{1/2}} = 2^{1/2}\delta_1 \ , \tag{42}$$

and

$$\rho^2 = \left[\frac{u_{0e}(1-5\beta/2)}{w_{0e}}\right]^2 \ , \tag{43}$$

We convert Eqs. (36) and (37) to the succinct form

$$\frac{d}{dx}x\frac{dP}{dx} = -e^{(P+Q)} \ , \tag{44}$$

$$\frac{d^2Q}{dx^2} = -\alpha_0 e^{(P+Q)} \ . \tag{45}$$

where $x = r^2/\delta_0^2$, and $\alpha_0 = \delta_0^2/\rho^2$. Notice that the parameter ρ^2 is a dimensional measure of the ratio of the axial to the azimuthal current, while α_0 is dimensionless. Since δ_0 is the expected macroscopic length, $\alpha_0(\approx \rho^{-2})$ is a proper indicator of the relative strength of the azimuthal to the axial current. Interestingly enough, Eqs. (44) and (45) allow exact analytical solutions

$$P = -b\ln\left(1 + \frac{x}{b}\right) \ , \tag{46}$$

$$Q = \alpha_0 b^2 \ln\left(1 + \frac{x}{b}\right) \ . \tag{47}$$

from which, we can derive

$$B_\theta = 2(\pi p_0)^{1/2} \frac{x^{1/2}}{1+\frac{x}{b}} , \tag{48}$$

$$B_z = -2b(\alpha_0 \pi p_0)^{1/2} \frac{1}{1+\frac{x}{b}} , \tag{49}$$

$$J_z = \left(\frac{c p_0^{1/2}}{\pi^{1/2} \delta_0} \right) \frac{1}{\left(1+\frac{x}{b}\right)^2} , \tag{50}$$

$$J_\theta = -(\alpha_0 x)^{1/2} J_z , \tag{51}$$

$$g = \left(1+\frac{x}{b}\right)^{-b[(3\beta-2)/(5\beta-2)-\alpha_0 b]} , \tag{52}$$

$$\psi^2 = \left(1+\frac{x}{b}\right)^{[-2\beta b/(5\beta-2)]} , \tag{53}$$

where we have used the notation

$$h_0 \delta_0^2 = \left(\frac{\alpha_0}{\pi p_0} \right)^{1/2} , \tag{54}$$

$$b = \frac{1}{\alpha_0} - \frac{2}{\mu} , \tag{55}$$

and

$$\mu = \alpha_0 b . \tag{56}$$

To see the relationship of these solutions to the previous results,[1,2] we first express b in terms of α_0. Eliminating μ in Eqs. (55) and (56), and solving the quadratic, we find

$$b_\pm = \frac{1 \pm (1-8\alpha_0)^{1/2}}{2\alpha_0} . \tag{57}$$

Since α_0 and b are real, α_0 clearly must be in the range, $0 \leq \alpha_0 \leq 1/8$, and b then can be shown to be in the range, $2 \leq b \leq \infty$. Note that the $\alpha_0 = 0$ limit of b_- yields $b_- = b = 2$ which will exactly reproduce the solutions given in Refs. 1 and 2. We further note that, with the inclusion of J_θ, the scale length b increases and β, required to have decaying g and ψ, also increases. These parameters have the values of $b = 2$, and $\beta > 2/3$ in the earlier

result.[1,2] For example, $\alpha_0 = 1/8$ gives $b = 4$, and $\beta > 2$ is required to have decaying density and temperature profiles.

The model equations (36) and (37) do not contain any external magnetic field but deal only with the self consistent fields created in the plasma. Note that a uniform magnetic field in the $\hat{z}$ direction can be easily incorporated by redefining Q to include a term linearly proportional to x. The model equations remain unchanged with this transformation and the same solutions hold. However a more realistic situation is one in which the external field is created by coils at the boundary. This situation can be modeled with a current

$$J_\theta^{\rm ext} = J_0 r_c \delta(r - r_c) \ , \tag{58}$$

which when incorporated modifies Eqs. (36) and (37) to

$$\frac{d}{dx} x \frac{dP}{dx} = -e^{(P+Q)} \ , \tag{59}$$

and

$$\frac{d^2Q}{dx^2} = -\alpha_0 e^{(P+Q)} + \frac{\alpha_1}{x_0^{1/2}} \delta(x - x_0) \ , \tag{60}$$

where $\alpha_1 = 2\pi J_0 h_0 r_c^2 \delta_0 / c$, $x_0 = r_c^2/\delta_0^2$, and Q is now defined to be $Q = -h_0 r A_\theta = -h_0 r(A_\theta^s + A_\theta^{\rm ext})$, where A_θ^s and $A_\theta^{\rm ext}$ refer to the self-consistent and external parts of the vector potential. Equations (59) and (60) need to be solved numerically with appropriate boundary conditions. For this purpose, it is more convenient to write them in the form

$$\frac{d}{dx} x \frac{dP}{dx} = -e^{(P+Q_s+Q^{\rm ext})} \ , \tag{61}$$

and

$$\frac{d^2Q_s}{dx^2} = -\alpha_0 e^{(P+Q_s+Q^{\rm ext})} \ , \tag{62}$$

where $Q_s = -h_0 r A_\theta^s$, and $Q^{\rm ext} = -h_0\, r A_\theta^{\rm ext}$ satisfies the equation

$$\frac{d^2Q^{\rm ext}}{dx^2} = \frac{\alpha_1}{x_0^{1/2}} \delta(x - x_0) \ , \tag{63}$$

with the solution

$$Q^{\text{ext}} = \begin{cases} 0.5B_0 \left(\dfrac{\alpha_0}{\pi p_0}\right)^{1/2} x \ , & x \le x_0 \ , \qquad (64a) \\ 0.5B_0 \left(\dfrac{\alpha_0}{\pi p_0}\right)^{1/2} x_0, & x \ge x_0 \ . \qquad (64b) \end{cases}$$

We consider the situation where the plasma edge is a conducting wall, so that $B_n = 0$, where B_n is the normal component of the magnetic field. This implies that the toroidal flux ϕ_t is conserved, i.e., $\langle B_t \rangle = B_0$, where

$$\langle B_z \rangle = \frac{2\pi}{\pi r_p^2} \int_0^{r_p} B_z r dr = B_0 + \frac{2}{r_p} A_\theta^s(r_p) \ . \qquad (65)$$

Conservation of ϕ_t thus forces the boundary condition $A_\theta^s(r_p) = 0$, i.e., $Q_s(r_p) = 0$. We solve Eqs. (61) and (62) numerically with the following boundary conditions

$$P(x = 0) = 0, \quad P'(x = 0) = -1 \ , \qquad (66)$$

and

$$Q_s(x = 0) = Q_s(x = x_p) = 0 \ . \qquad (67)$$

Since we want to express all our results in terms of a minimum number of macroscopic plasma parameters, it is important that we impose additional constraints to limit the choice of solutions. It is natural to believe that stable and interesting equilibria should correspond to a minimum of the total energy

$$W = \pi \delta_0^2 \int_0^{x_p} \left[\frac{3}{2}\beta_0 e^{P+Q_s+Q^{\text{ext}}} + \left(\frac{B_z}{B_0}\right) + \left(\frac{B_\theta}{B_0}\right)\right] dx \ , \qquad (68)$$

where W is normalized to $2\pi R_0 B_0^2/8\pi$ with R_0 being the major radius, and $\beta_0 = 8\pi p_0/B_0^2$. The minimization is to take place with respect to α_0 (a measure of the ratio of the azimuthal to the axial current) and β_{p0} which represents the central plasma pressure. A typical plot of $B_z(B_\theta)$ is presented in Fig. 11(12). It is seen, that unlike the unconstrained solutions [(46) to (53)], these solutions can exhibit field reversal and thereby bear a close resemblance to

'relaxed' states of reversed field pinches. 'Relaxed' states have been extensively discussed in the literature[3] within the context of the ideal fluid model. Our equilibrium solutions can be viewed as a kinetic analog of such states, with finite pressure and finite pressure gradients. For our simple model, we can also construct a $F - \Theta$ diagram to map the reversed field regime, where $F = (B_z/B_0)_{r_p}$ and $\Theta = (2I_z)/(cr_pB_0)$ with I_z being the total current in the $\hat{z}$ direction. An example of a $F - \Theta$ plot, showing the field reversal ($F = 0$) at $\Theta = 1.57$, is shown in Fig. 13. Notice that in this paper, we are simply attempting to investigate the scope of constrained Vlasov-Maxwell equilibria; we do not make any detailed comparison with pinch experiments.

VI. Discussion

In this paper, we have considered two kinds of improvements on exact solutions of the Vlasov-Maxwell system and tried to understand their significance for modelling realistic laboratory plasmas. The first kind of improvement lies in extending previously obtained one dimensional solutions of a simple Z pinch model to obtain two dimensional exact solutions. These solutions display a great deal of interesting structure. For the $m = 1$ case, the equilibrium magnetic surfaces are shifted circles, where the shift is controlled by a parameter $\epsilon (0 \leq \epsilon < 1)$. The self consistent plasma profiles (density and temperature) also display corresponding shifts in their peak values. The $m \geq 2$ equilibria display magnetic surfaces with chains of islands and separatrices, but have a singularity at the origin. All these equilibrium states (with self consistent plasma profiles) can play a significant role in understanding a wide variety of laboratory plasma situations.

Fluid analogs of the $m \geq 2$ states have been considered in the past for stability studies of magnetic islands around mode rational surfaces in tokamaks,[5] or Kelvin-Helmholtz vortex formation in cross-field plasma sheaths.[6] Our kinetic states could represent a better equilibrium model for many such situations.

Our second direction of improvement has been toward incorporation of an azimuthal current in the pinch model to arrive at a better representation of laboratory devices like the reversed field pinches. Restricting ourselves to one dimensional cylindrical geometry, we have once again been able to obtain exact analytical solutions of the Vlasov-Maxwell system. These equilibrium states, which have well behaved monotonic plasma profiles, do not exhibit any field reversal. However, introduction of appropriate physics, like a uniform external axial magnetic field (created by currents at the boundary), and conducting boundary walls (imposing toroidal flux conservation) lead to a more realistic model; the total toroidal magnetic field B_z can now change sign near the plasma edge. These equilibrium states resemble the 'relaxed' states of reversed field pinches and can be viewed as the kinetic analog of such states with finite pressure and finite pressure gradients. Although a detailed analysis and further refinements are necessary to establish a proper correspondence with the experiment, and also with the existing 'relaxed' equilibrium states, the present solutions demonstrate once again the power and simplicity of the Vlasov approach. Further refinements in the model are in progress.

Acknowledgments

This work was supported by the U.S. Department of Energy Contract No. DE-FG05-80ET-53088, and also by the International Centre for Theoretical physics.

References

1. S.M. Mahajan, Phys. Fluids B **1**, 43 (1989).

2. S.M. Mahajan and W.Q. Li, Phys. Fluids B **1**, 2345 (1989).

3. J.B. Taylor, Rev. Mod. Phys. **58**, 741 (1986).

4. Fadeev *et al.*, Nucl. Fusion **5**, 202 (1965).

5. J.M. Finn and P.K. Kaw, Phys. Fluids **20**, 72 (1977).

6. K. Theilhaber and C.K. Birdsall, Phys. Rev. Lett. **62**, 773 (1989).

Figure Captions

1. Magnetic surfaces for the azimuthal mode number $m = 1$ at $\epsilon = 0$. The surfaces are centered at the origin.

2. Plot showing the displacement of the center of the magnetic surfaces; maximum displacement is $X \simeq -1$, for $m = 1$ at $\epsilon = 0.7$.

3. Centers of the magnetic surfaces shift back towards the origin for $m = 1$ at $\epsilon = 0.9$.

4. Numerical plots of the plasma energy versus the normalized radius r/δ_1 for $m = 1$ at different ϵ. For larger ϵ, the plasma is displaced from the center.

5. Numerical plots of the magnetic energy versus the normalized radius r/δ_1 for $m = 1$ at different ϵ. For larger ϵ, the magnetic energy forming a well near the peak of the plasma energy [Fig. 4] is clearly shown.

6. Magnetic surfaces for $m = 2$ at $\epsilon = .551$. The magnetic islands and $\times$ points are clearly shown. The crowded contours near the center represent that the solutions are singular at the origin.

7. Numerical plots of the magnetic surfaces for $m = 3$ at $\epsilon = .6759$. Similar to Fig. 6, the contours display the islands, X points, and a singularity at the origin.

8. Numerical plots of the magnetic surfaces (similar to those of Figs. 6 and 7) for $m = 10$ and $\epsilon = .662$.

9. An example of the plasma energy versus the normalized radius r/δ_1 for $m \geq 2$ at different ϵ. The plasma has completely moved away from the center, showing that the solutions are singular at the origin.

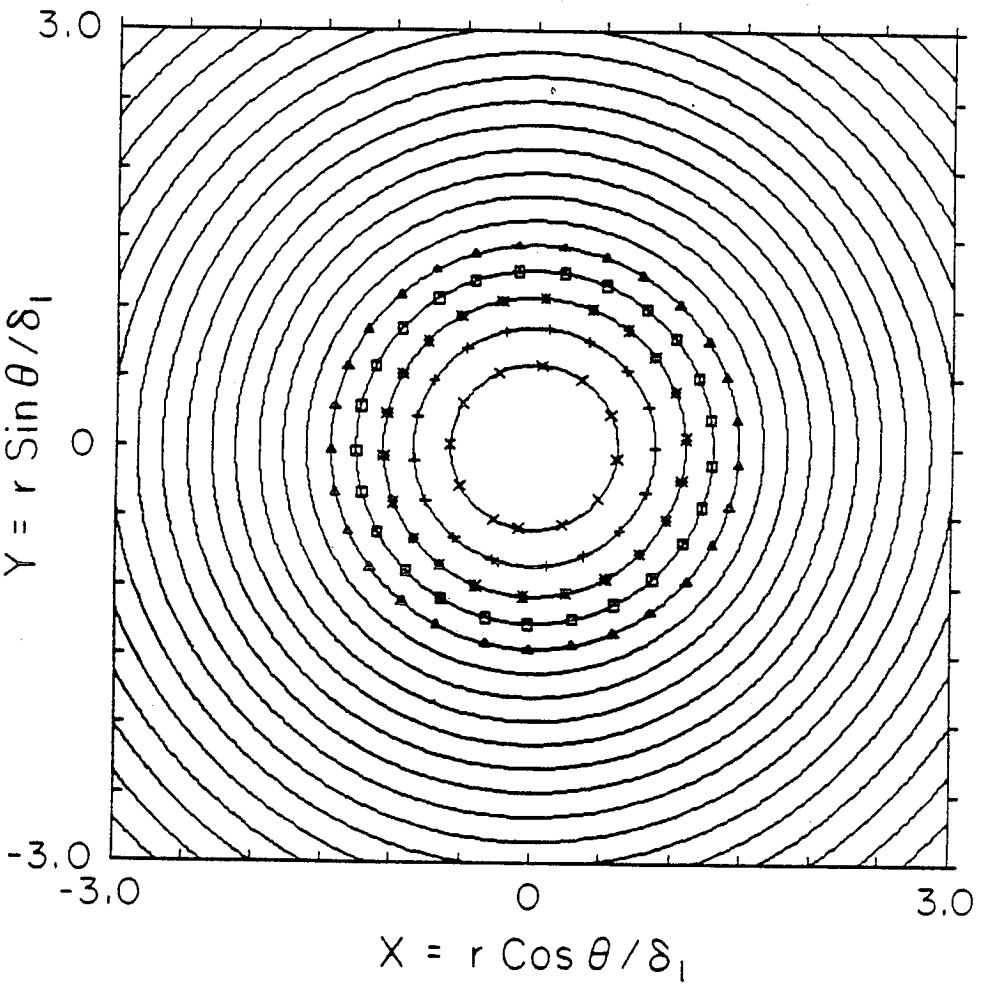

Fig. 1

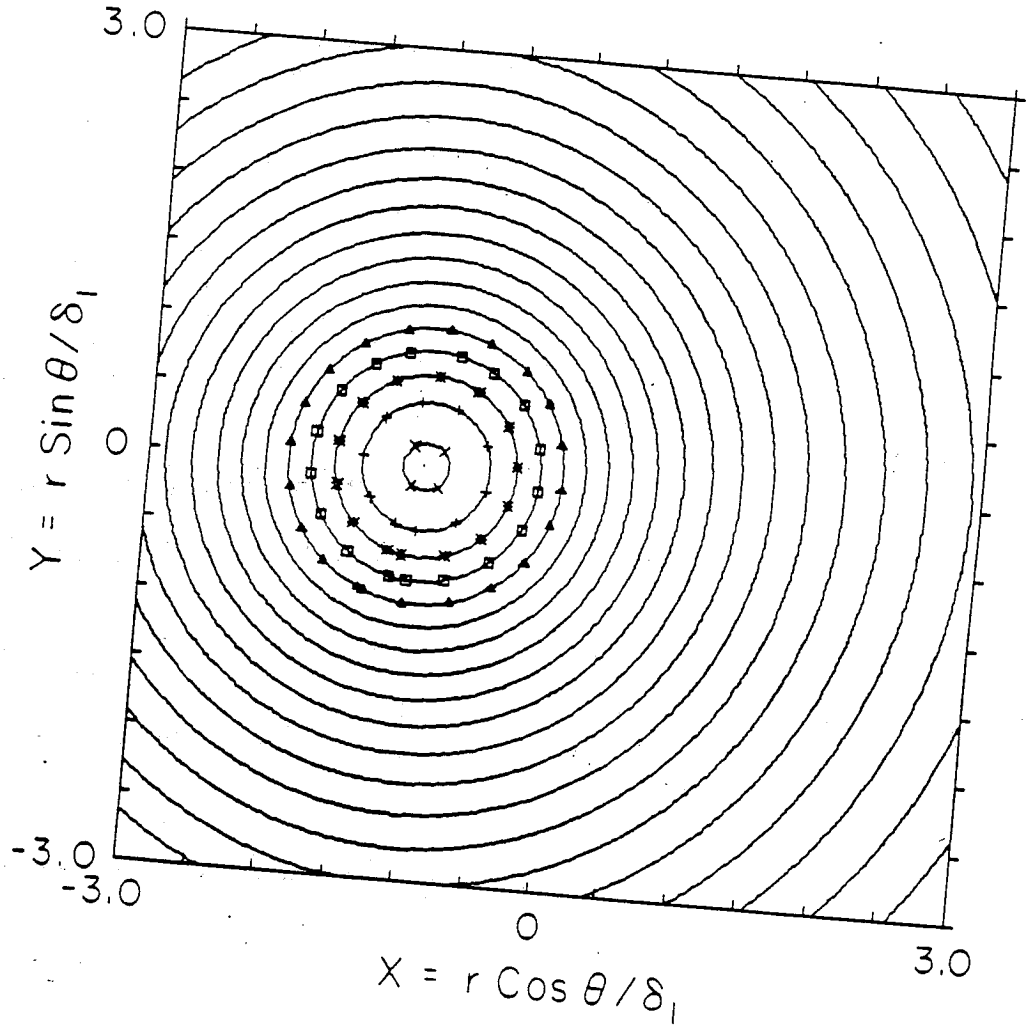

Fig. 2

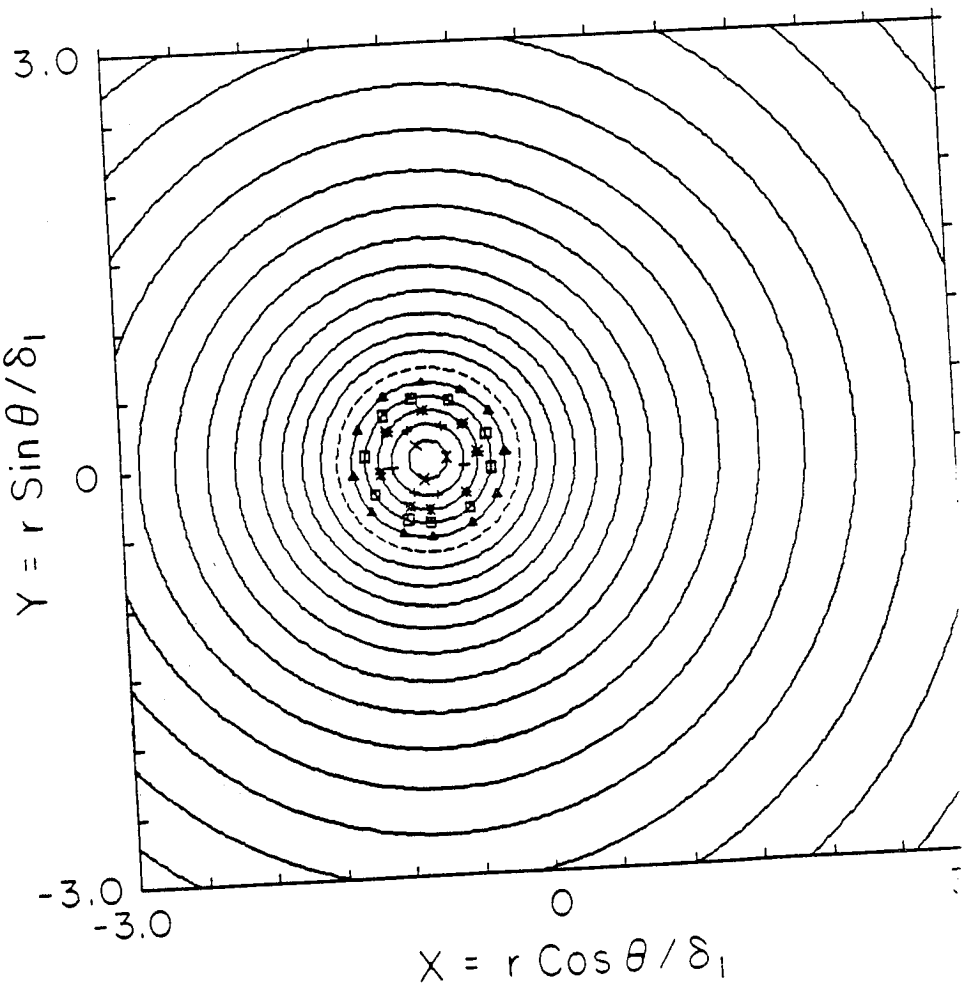

Fig. 3

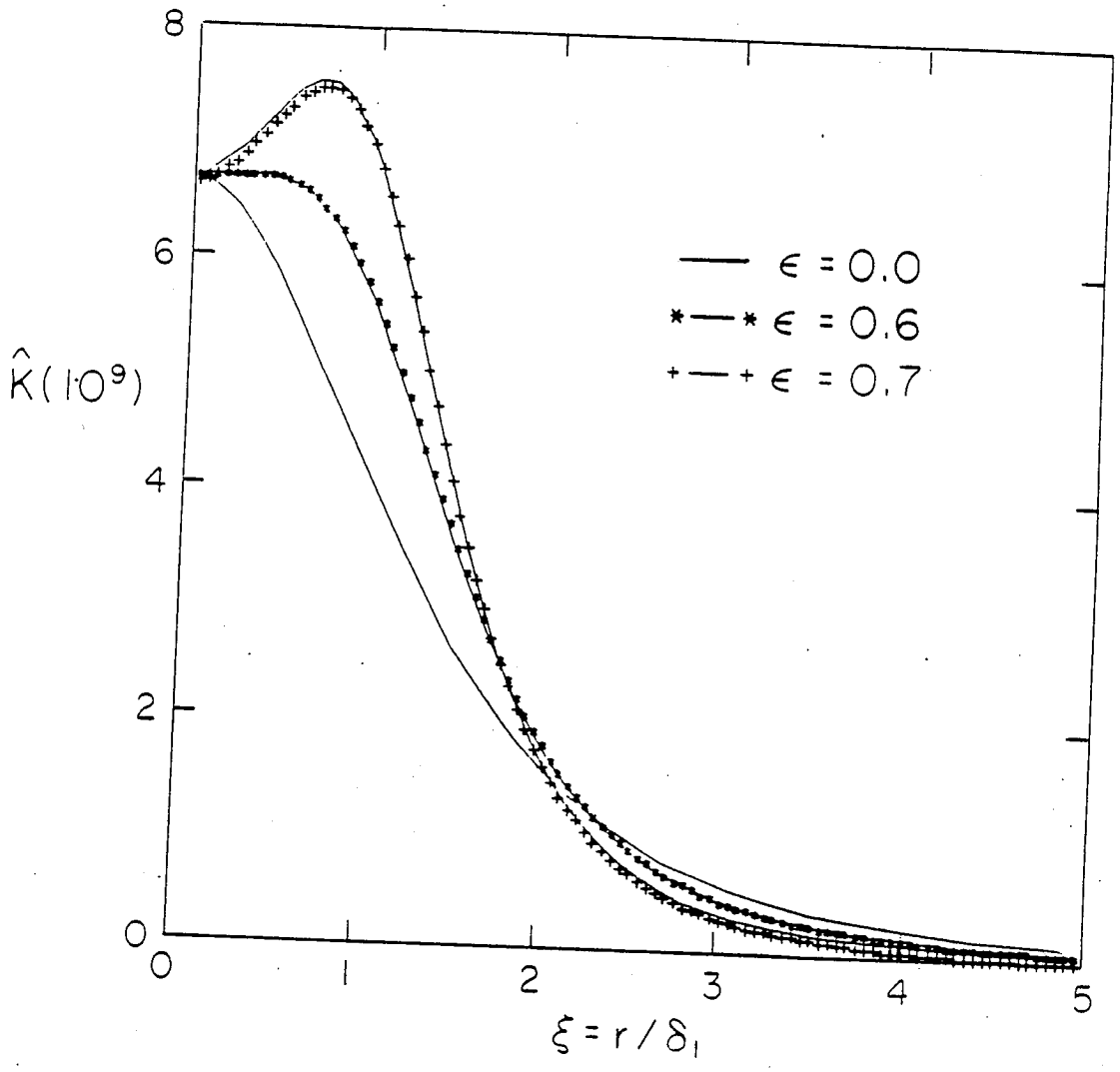
8
6
4
2
0
0
1
2
3
4
5
$\hat{K}(10^9)$
$\xi = r/\delta_1$
$\epsilon = 0.0$
$\epsilon = 0.6$
$\epsilon = 0.7$

Fig. 4

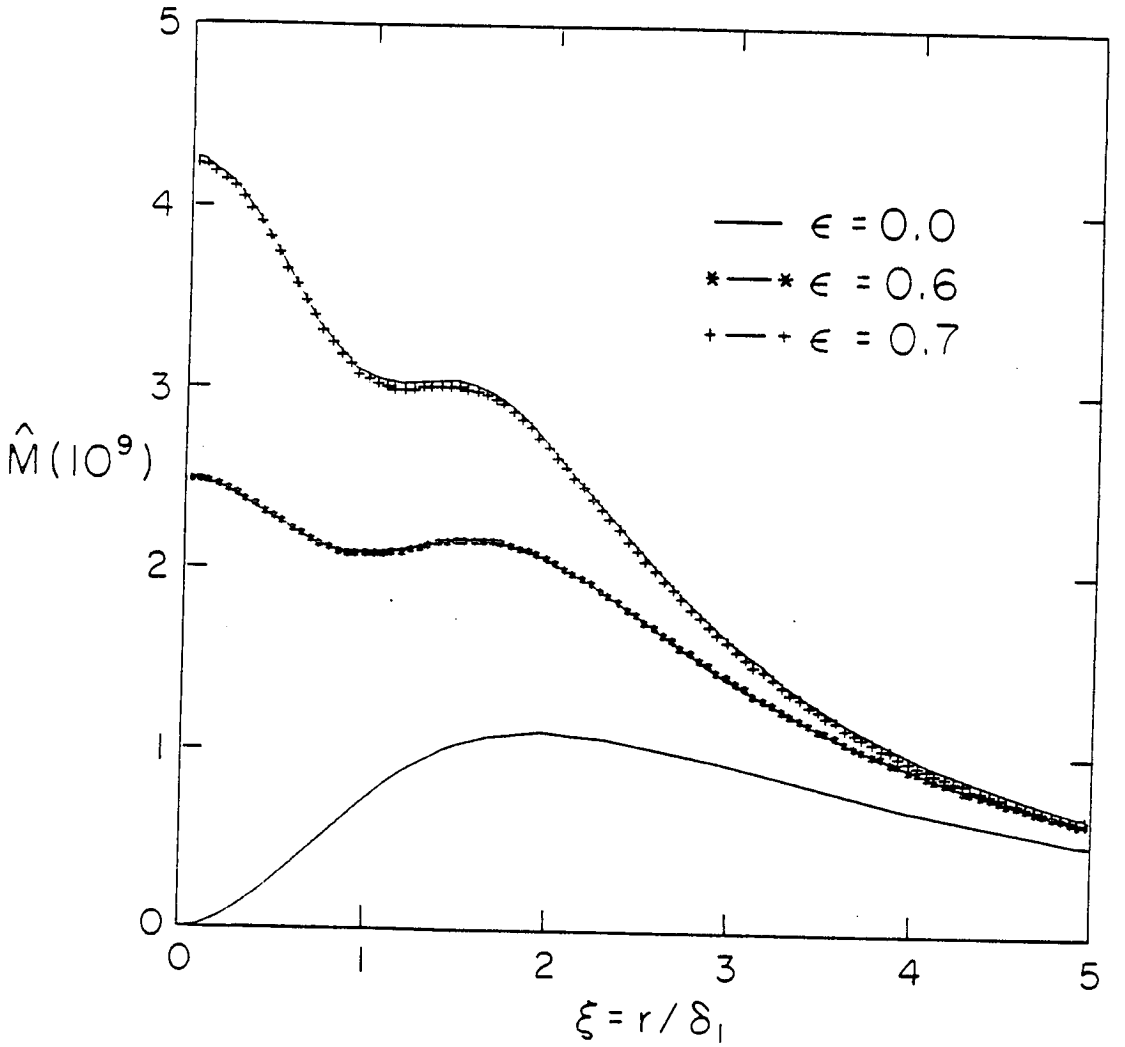
5
4
3
2
1
0
0
1
2
3
4
5
$\hat{M}(10^9)$
$\xi = r/\delta_1$
$\epsilon = 0.0$
$\epsilon = 0.6$
$\epsilon = 0.7$

Fig. 5

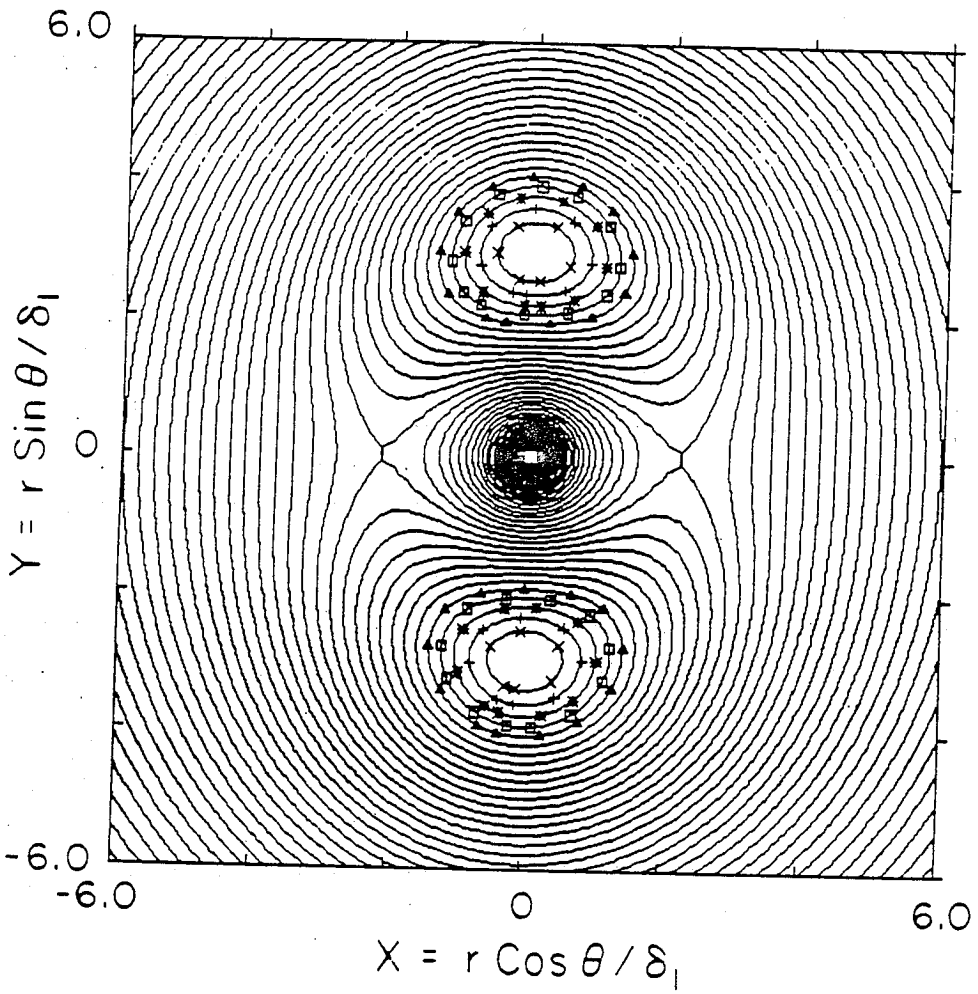

Fig. 6

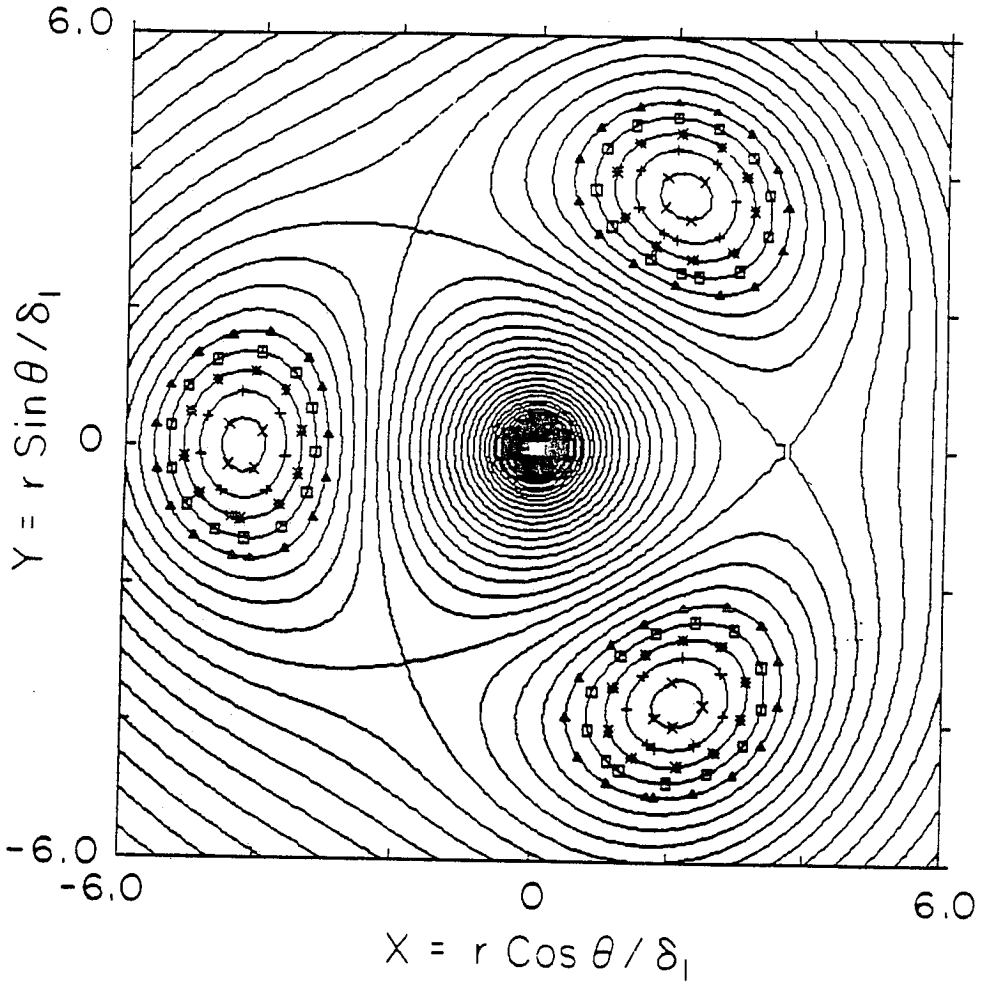

Fig. 7

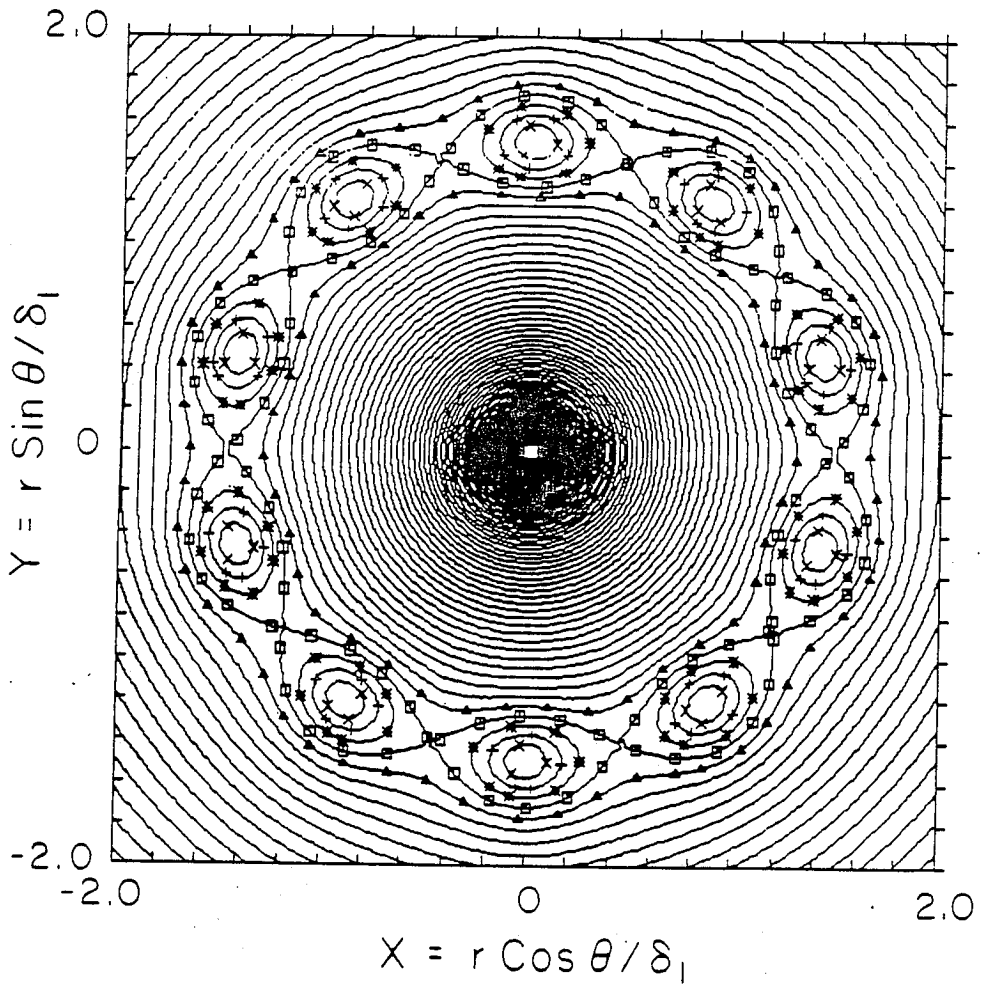

Fig. 8

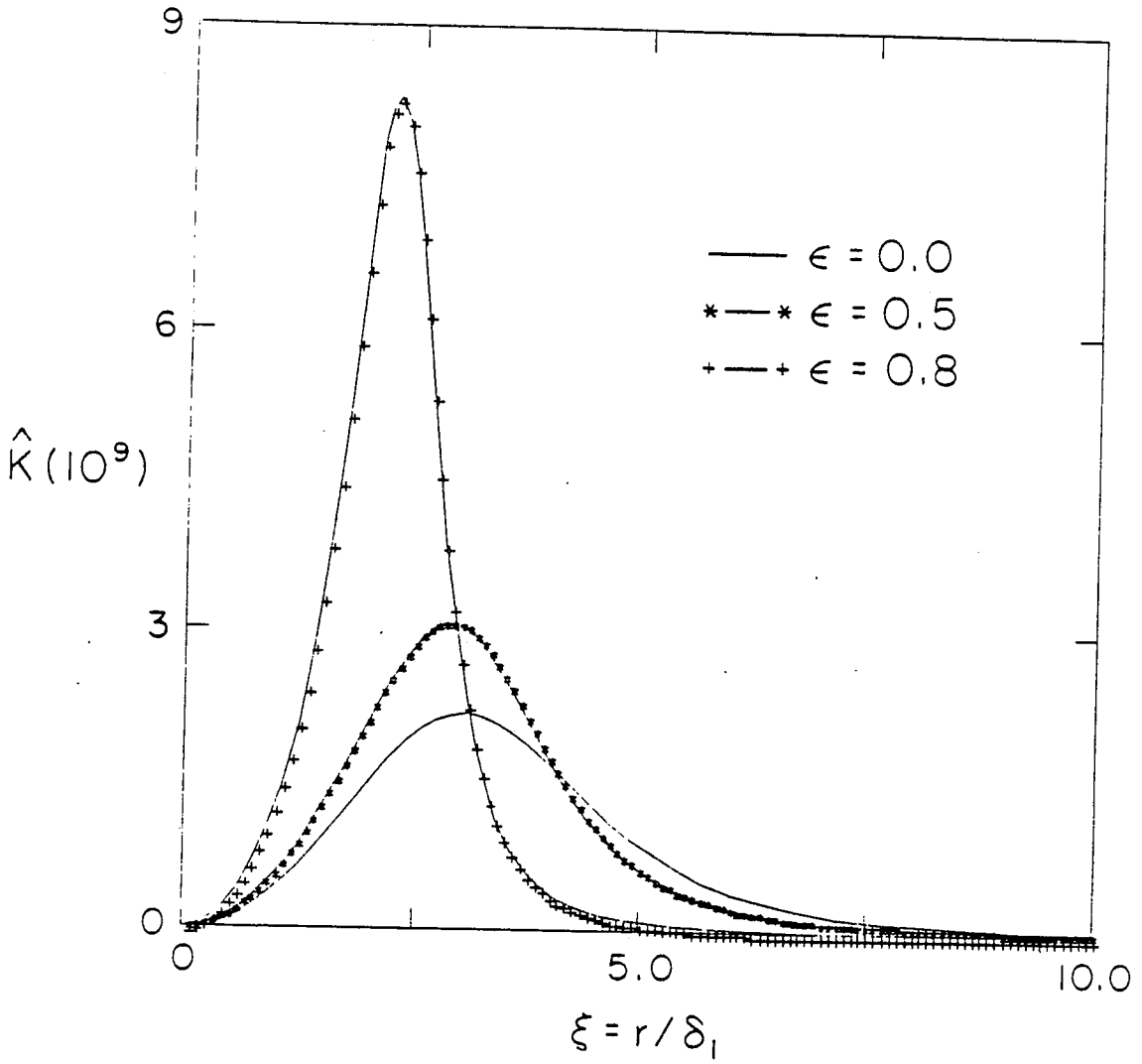
9
6
3
0
0
5.0
10.0
$\hat{K}(10^9)$
$\xi = r/\delta_1$
$\epsilon = 0.0$
$\epsilon = 0.5$
$\epsilon = 0.8$

Fig. 9

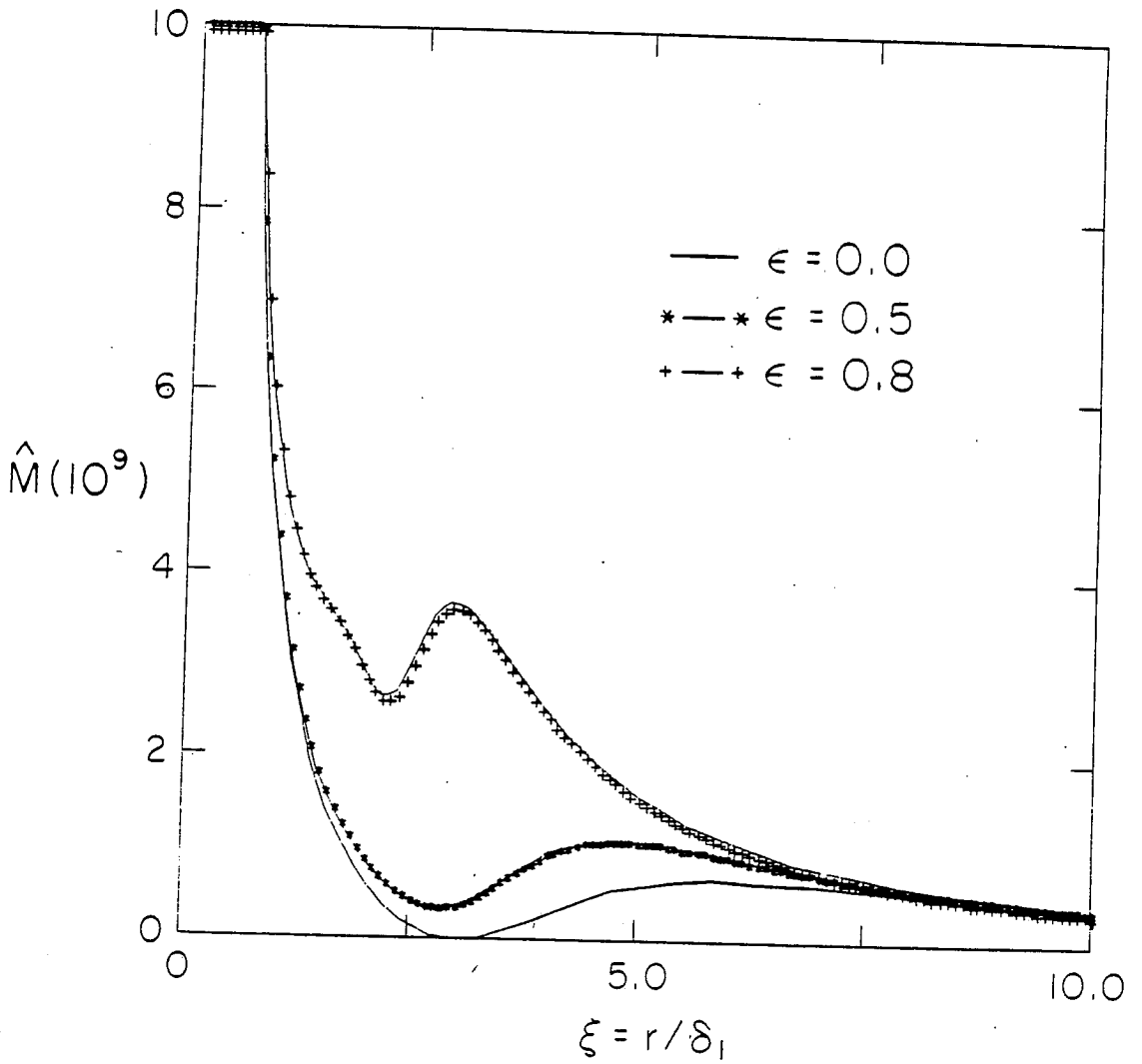
10
8
6
4
2
0
0
5.0
10.0
$\hat{M}(10^9)$
$\xi = r/\delta_1$
$\epsilon = 0.0$
$\epsilon = 0.5$
$\epsilon = 0.8$

Fig. 10

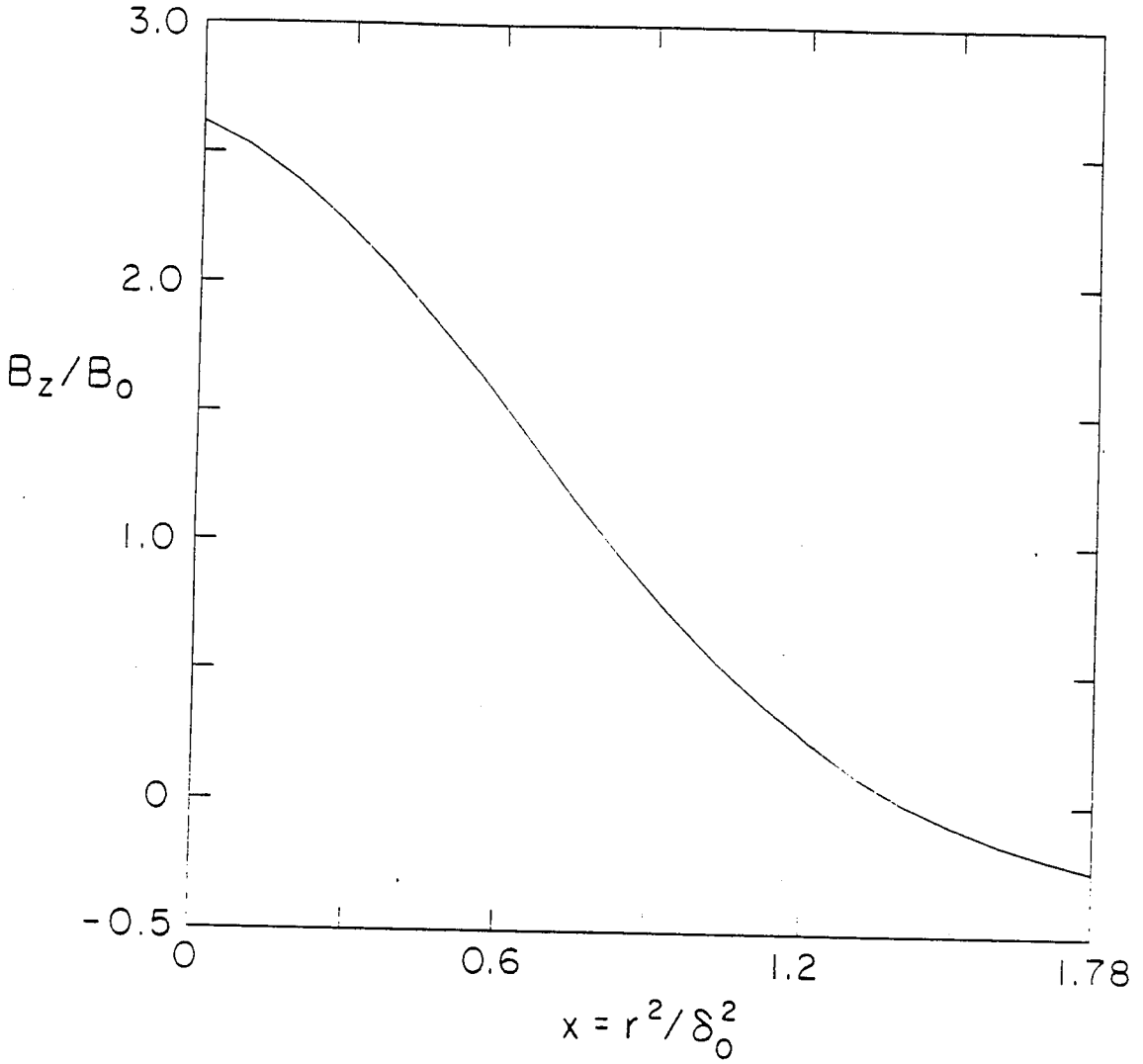

Fig. 11

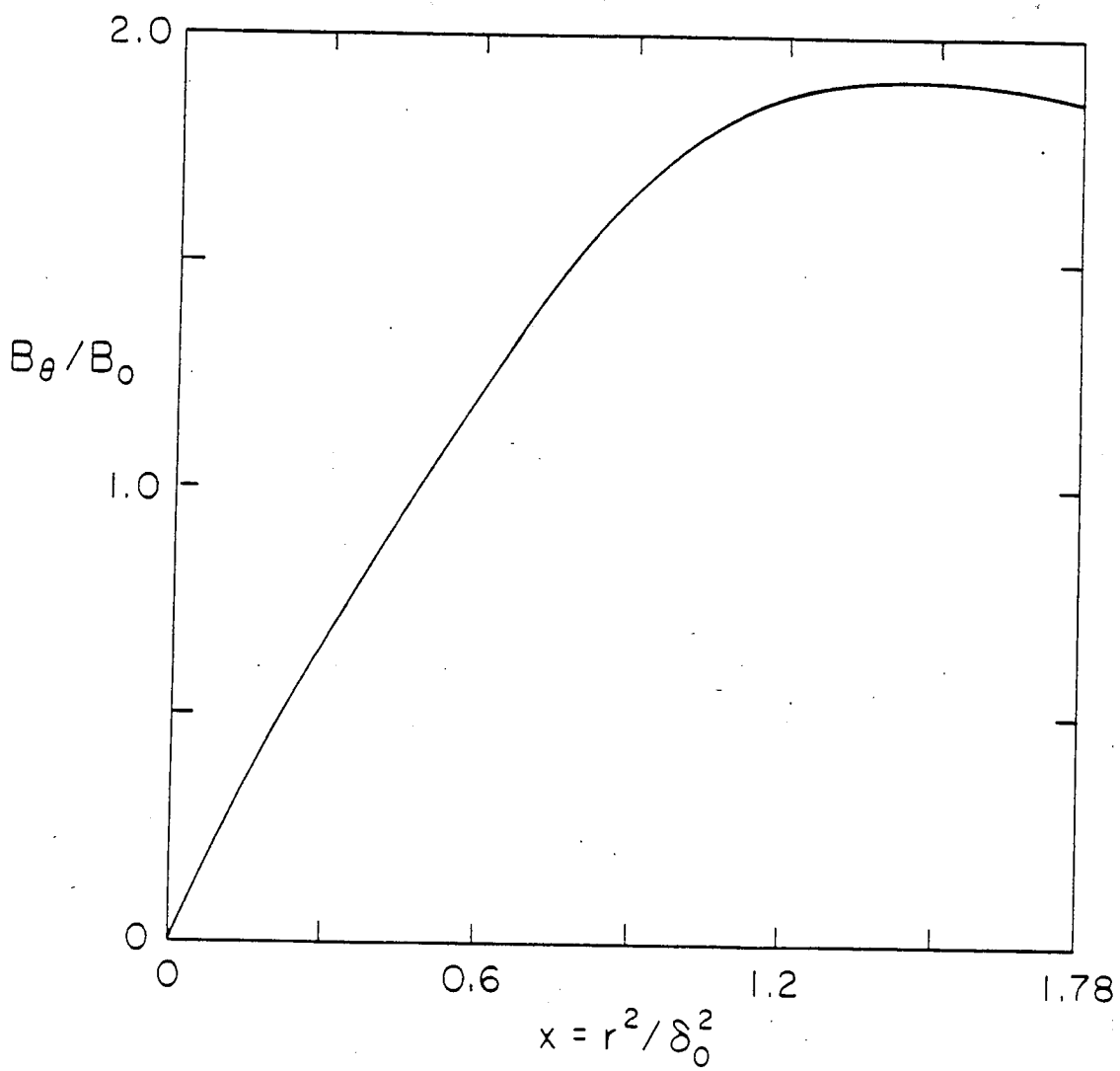

Fig. 12

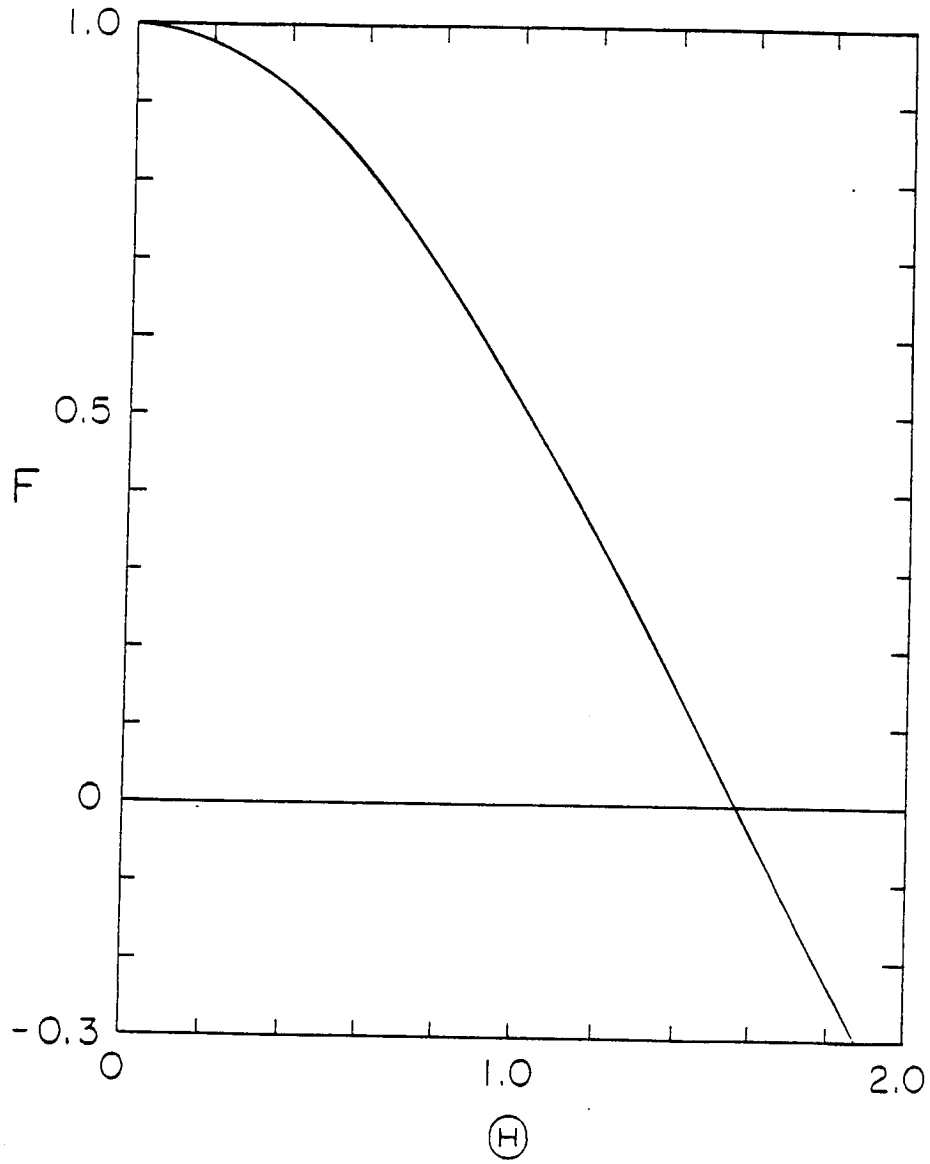

Fig. 13